AIAA-2001-1197

DISTRIBUTED LOCALIZED SHAPE CONTROL OF GOSSAMER SPACE STRUCTURES

Dimitry Gorinevsky, Honeywell Laboratories, Cupertino, CA 95014
Tupper Hyde, Honeywell Space Systems, Glendale, AZ 85308
Cleopatra Cabuz, Honeywell Laboratories, Plymouth, MN, 55441

Keywords: spacecraft, gossamer, large lightweight apertures, control, vibration control, wavefront control.

Abstract

Future earth science, space science, exploration, and reconnaissance space missions will require increasingly large and lightweight apertures. Although they have low areal mass density, the deployed aperture structures must capture and hold a surface figure to a fraction of a wavelength in the presence of thermal, slew, and vibration disturbances. Active control of surface figure is a key technology for the success of gossamer space structures. Less than several hundred actuators could be still controlled by using a centralized computing element. If, however, there are thousands of actuators distributed in the surface, the control hardware and computations should be distributed as well. This paper discusses how an efficient control of a gossamer structure shape can be achieved using large distributed actuator arrays. Advanced algorithms using only local information about errors and actuation for collocated and neighboring positions in each of the distributed computational elements allow achieving required control performance. A gossamer structure with built-in distributed actuators, sensors, and computational elements can be made scalable to a very large size. Of course, integrating thousands of actuators, in a structure in a practically affordable way requires actuators are mass producible. MEMS technologies based on electrostatic actuation and implemented on compliant plastic substrates, represent a highly attractive proposition thanks to their very low areal density. A distributed surface control approach is a key enabler for future gossamer space apertures.

Gossamer Space Apertures

To meet the future mission demands for large lightweight space apertures, gossamer structures will be required with ever decreasing areal densities [1,2]. At first these will be accomplished with "rigid" deployable systems, followed by larger, more flexible deployables, shell structures, inflatables, and membranes. The surface precision of these radio frequency (RF) and optical (IR/visible/UV) reflectors will remain at a fraction of the wavelength regardless of dimension of the aperture. To take advantage of the ability to collect low signals, one requires large areas; to get high resolution, one requires large aperture dimensions (or baselines for sparse aperture instruments). An example large RF aperture is the 5 meter diameter TDRSS mesh deployed antenna with a surface precision of half a millimeter and mass of 24 kg. In the optical, it is the 2.4 meter Hubble Space Telescope (HST) primary mirror with an effective surface precision (after corrective optics) of 20 nanometers and mass of about 400 kg. HST corrects only for piston, tip and tilt (3 actuators). In the next decade, the Next Generation Space Telescope (NGST) will be designed to use deployed panels and perhaps hundreds of actuators to control a mirror surface to about 50 nanometers across its 8 meter diameter with an areal density of 10 kg/m^2.

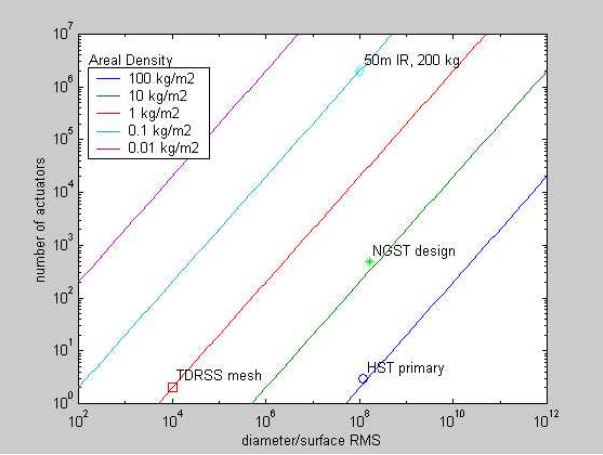

Figure 1: Number of actuators required to hold surface precision versus aperture size and areal density (with several known or predicted point designs plotted). A Gossmaer structure such as a 200 kg, 50 meter IR reflector would require millions of actuators.

Future space apertures will be increasingly called upon to provide diffraction limited surface figures at ever increasing dimensions. Large, lightweight (gossamer) apertures of future space missions will not meet there figure precision passively upon deployment due to thermal effects, gravity unloading, materials uncertainty, and mechanical precision

tolerances. Actuators can undo these effects and adapt the aperture figure to the desired shape. Large gossamer apertures for future space missions will have diameters of several tens of meters and much lower areal weight. Many hundred thousands or millions of actuators will be needed to compensate for the main reflector figure error [3]. The number of actuators required depends on the stiffness and stability of the passive structure and the figure precision required. Figure 1 shows an estimate of the number of actuators required versus aperture size and areal density.

Maintaining the figure despite deployment errors and thermal and other low-bandwidth disturbances inherent to such spacecraft operation requires closed-loop control of all these actuators. Control of very large number of actuators becomes possible by making the control computing physically distributed on the membrane substrate. The real-time control of each actuator will be localized using information from collocated and neighboring sensors and actuators only. Such membranes can be scaled to a very large size with millions of actuators, each controlled independently of all but several neighbors.

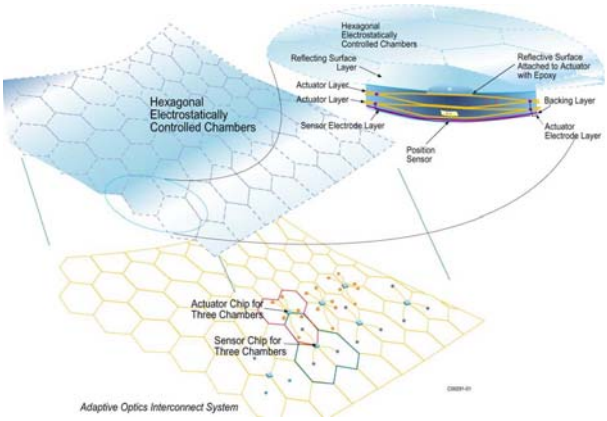

Figure 2. Multifunctional adaptive membrane concept.

Such apertures would be enabled by the mutifunctional adaptive membrane technology. A mutifunctional adaptive membrane envisioned in Figure 2 will have built-in actuators, sensors, and controls. If produced in large quantities, the membrane can be made relatively inexpensively. It can be used as a subsystem when designing different missions. It can be used within lenticular inflatable space RF telescope antennas [4], mesh structures [5], and other spacecraft concepts [6]. This paper describes the technology developments in Honeywell that would ultimately lead toward manufacturing of such membranes as a potential product line. The key technologies discussed below are lightweight plastic actuators and active distributed surface controls. Another key technology is the real time sensing of the membrane figure error. The figure metrology issues are not discussed in this paper because of the size constraints.

The unique polymer electrostatic actuator technology was developed by Honeywell under several DARPA contracts. Some of the actuator design approaches are described in the next section. This technology could provide an actuator force of 1 N/cm^2 over 100 μm displacement with an actuator cell size of 1-3 cm, and thickness of folded membrane of 100-200 μm. The areal density of such membrane would be less than 0.2 kg/m^2.

The system design of a multifunctional membrane follows from the required control functionality. The first task of the active surface control is to initially figure the aperture after deployment. Once this initial "capture" of the figure is accomplished, the bandwidth of the surface control depends on the time dependence of the disturbance sources. The orbit and sun shading might be benign enough to allow only periodic re-figuring without any significant loss of mission time. In earth orbit, or where significant attitude slewing is required, the figure control will be required to be active during use of the aperture. Thermal time constants would be on the orbital time scale, slew acceleration induced disturbance have time constants based on vehicle agility, and spacecraft bus vibration disturbances are at many frequencies up to hundreds of Hz. Passive natural structural frequencies of a gossamer aperture will be very low and get dense quickly in frequency. Careful design of the active surface control is a must. For some disturbances, control authority over many surface modes of high spatial and temporal frequency is required while avoiding destabilizing effects of the disturbances outside of dynamical or spatial bandwidth of the controller. Design of distributed decentralized control architecture satisfying the above requirements is discussed later in this paper.

Actuator Hardware Concept

A large aperture gossamer structure with an actively controlled surface places tough constraints on the types of materials and actuation mechanisms that can be used. Our experience indicates that an electrostatic mechanism is very adequate for building large 2-D and 3-D arrays of low-weight, low-power actuators [7,8,9,10]. An electrostatic actuator is essentially a capacitor. The actuating elements are the electrodes and the dielectric layer. The power consumption of one actuator node in a static condition would be in the microwatt range and depends on the leak in the dielectric material. During switching, the power scales linearly with the actuation frequency.

While electrostatic actuation is generally known as a high-voltage/low-displacement mechanism, our design provides a remarkable improvement, resulting in increased strokes (hundreds of microns) and low voltages (between 50 and 150 V). The enabling element in our actuators is a rolling contact, which allows spatial separation of the maximum force and maximum displacement. The force responsible for the movement is produced at the rolling contact of the actuator while the maximum displacement is obtained at a different location, which could be the free end of a flap (Fig. 2a [10]) or the center of a buckled diaphragm (Fig. 2c [8,9]). We have demonstrated valves, pumps, and musclelike structures based on rolling contact electrostatic actuators, all of them using plastic substrates such as a Kapton film [8,9].

The actuating elements of a typical electrostatic actuator using 100-Å-thick aluminum electrodes and 1-μm organic dielectric have an areal density of about 1.5 g/m^2. In addition to the actuating elements, the actuator structure might also include stronger and thicker (10 to 25 μm) polymeric films.

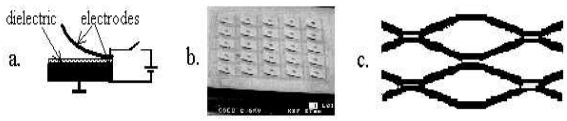

Figure 2. (a) Concept of a rolling-contact electrostatic actuator; (b) SEM photograph of Honeywell silicon micromachined actuator array [10]; (c) cross section of a multilayer PolyMEMS electrostatic actuator for linear motion actuation [8,9].

Different actuator configurations can be used for the fine and coarse control of the reflector surface. For the fine control of the surface a single layer of the actuator shown in Figure 2c can be used. Slight modifications in the actuator's structure can ensure bidirectional actuation. On the other side, a multilayer PolyMEMS actuator [9] (Fig. 2c) can produce midrange displacements. A 5-mm total travel could be achieved for a structure having 50 actuation layers, which in the folded condition will have a thickness of about 2.5 mm. With 12.5-μm (0.5 mil) films, the areal density of such a structure will be about 1.75 kg/m^2. Using thinner films could conceivably reduce the membrane weight even more. The fine and coarse actuators could be combined as different layers of a multilayered membrane.

The same principle of rolling contact electrostatic actuation on plastic substrates can be used to produce very light and simple pumps that could be used in a deployable configuration using pneumatic actuation. Such a pump, called the Double Diaphragm Pump is described below [11].

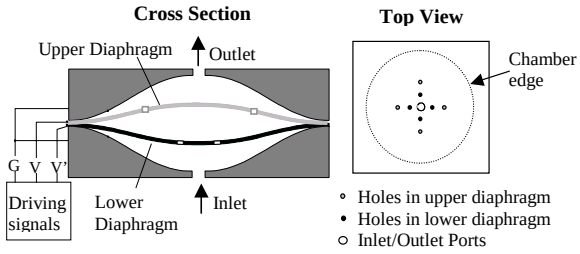

Figure 3. Left: Schematic structure of the Dual Diaphragm Pump (DDP). Right: Relative placement of the diaphragm through-holes and of the inlet/outlet ports.

Figure 3, left, shows the schematic structure of the DDP. The pump consists of a chamber and two thin diaphragms. Each surface of the pump chamber and of the two diaphragms has a very thin metal electrode covered with a dielectric. The diaphragms have several through holes, which are non-coincident between them and non-coincident with the inlet and outlet ports (Figure 3, right). When either diaphragm is fully deflected and electrostatically clamped to the upper or lower wall of the pump chamber, it closes the corresponding inlet/outlet port. When the two diaphragms are clamped together, they move as a single sealed diaphragm, pushing the gas in the desired direction. The electrodes from the upper and lower chamber walls are connected together to the electrical ground. The electrodes on the two sides of each diaphragm are connected together, resulting in the three electrical connections shown in Figure 3, left. The operation has three phases, shown in Figure 4.

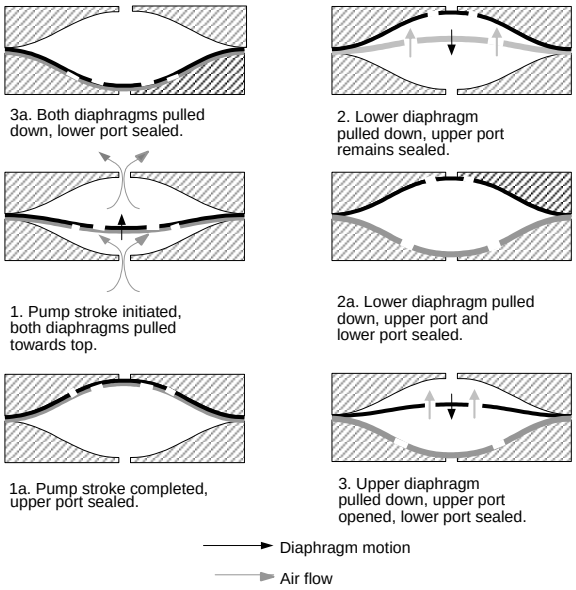

Figure 4. Operation of the Dual Diaphragm Pump

At the end of phase 3 both diaphragms are clamped to the lower wall of the chamber. This is achieved by applying a potential V to the lower diaphragm, while the upper diaphragm is connected to ground. In phase 1 the potential V is switched from the lower to the upper diaphragm, and the lower diaphragm is placed at ground. In this way, the diaphragms continue to be electrostatically clamped together, sealing each other's holes, but they start to move toward the upper chamber wall. During this phase, the gas in the chamber is pushed out through the outlet, and at the same time, the gas back-fills the chamber through the inlet port. At the end of phase 1, both diaphragms have touched the upper wall of the chamber, pushing out the entire volume of gas in the chamber and sealing the outlet. In Phase 2 both diaphragms are connected at the driving potential V. This causes them to separate and the lower diaphragm moves toward the lower chamber wall. Because the diaphragm has through-holes with a flow impedance smaller than that of the inlet port, no gas is pushed back through the inlet. The lower diaphragm is fully clamped to the lower chamber wall, sealing the inlet. In phase 3, the upper diaphragm is connected to ground, separating it from the upper wall and attracting it to the lower diaphragm. As in the previous step, because of the relative flow impedances of the diaphragm holes and of the outlet port, the diaphragm moves through the chamber without producing a net gas intake at the outlet. At the end of phase 3 both diaphragms are clamped to the lower wall, and the 3-phase cycle can now re-start. The pump has essentially zero dead-space and provides perfect rectification. The pumping rate has been measured in both directions for all the frequencies and driving voltages. Perfect symmetry in pumping is achieved. The change in pumping direction can be computer controlled. Any flow pattern (rate and direction) can be easily generated. The pressure-head measured for the current design of the Dual Diaphragm Pump is about 0.4psi. Shallower chambers could be used in the applications where higher pressure heads are required. The power consumption of the pump at maximum flow is about 8mW. The power consumption for the pump scales linearly with the driving frequency and quadratically with the driving voltage.

Figure 5 illustrates one possible concept of inflatable actuators based on electro-pneumatic control. The gas could be moved from one side of the central membrane to the other through the rolling action of the lower membrane. While extremely simple, such an approach requires relatively thick membranes to prevent gas leak. Individual control of displacement in each pixel could be achieved through the use of active pumping, based on light devices such as the dual diaphragm pump. Though very fine patterns of the figure error cannot be controlled this way, such actuators could compensate for large figure errors that gradually accumulate over the reflector size. This design would be most applicable to space inflatables, such as lenticular RF antennas [4], where the membrane already has to contain a pressurized gas.

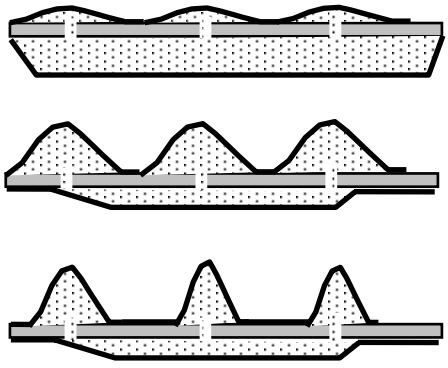

Figure 5. Multifunctional membrane with combined electrostatic-pneumatic actuation.

Distributed Localized Control of Large Actuator Arrays

The distributed localized control technology we are developing is applicable to a broad variety of adaptive membrane designs using different actuation and sensing principles. The entire membrane surface will be subdivided into identical cells, each containing one or more sensors and actuators. Each cell or cluster of neighboring cells will have a control module. The control for each cell is computed as a weighted sum of past control and sensor measurement errors for it and several neighboring cells. These real-time distributed localized control calculations are straightforward and can be realized in simple control module hardware. Design and analysis of such a controller, however, goes beyond standard control technology. The technology for the membrane system modeling, analysis, and control design is based on multidimensional systems theory and discussed below. To enable the control computations, each distributed control module will exchange data with its neighbors.

An active surface of a gossamer structure with embedded actuators, sensors, and computational elements represents an array control system**.** In such system variables, measurement, and control change in time and depend on spatial coordinates. Multidimensional signal processing for large sensor arrays has well-established theory and applications, especially in imaging. Yet, applied approaches to distributed localized control of large distributed actuator and sensor arrays are on the cutting edge of current control technology and are less well known. Our experience in control of arrays with hundreds of actuators and developed analysis tools is partially reflected in the literature [12-18].

Spatially distributed systems can be analyzed by modal decomposition such that the time dynamics of each mode is handled separately. For array systems, where identical multifunctional cells make a regular spatial grid, a modal decomposition is given by a spatial Fourier expansion [19]. This leads to spatial frequency analysis somewhat related to the frequency domain analysis used in standard control problems [20]. The multidimensional frequency analysis is applicable to very large array systems without any increase in complexity. This brings up the notion of spatial and dynamical bandwidth of the control system [13-18,21]. Recognizing spatial bandwidth limitations is related to the practice of discarding higher order spatial modes that are poorly controllable. The modal control, however, requires centralized computations with access to all measurements and actuator commands. The distributed array control is designed using only spatially localized information from near neighbor nodes in the array [17-18,21].

Many of familiar concepts of control design and analysis can be extended to array control systems. One key concept is control robustness to modeling error – both in description of dynamical and spatial response of the system [12]. For rigorous analysis of the robustness to models of both dynamical and spatial response of the system, we use a multidimensional extension [15,16] of structured singular value analysis (μ-analysis) [22]. This analysis is extended to allow for description of the boundary effects on the edges of the array. The robustness analysis is also used in the distributed localized control design to take into account the unmodeled flexible dynamics of the membrane.

Illustrative Example of Control Analysis

To illustrate our array control analysis technique, consider a one-dimensional model of a flexible space antenna reflector with a distributed active control of the shape. The reflector here is modeled as a thin beam with a bending stiffness C and free ends. The beam is subject to a longitudinal tension T. An array of actuators is uniformly spaced along the beam (Figure 6). Each actuator produces a controlled localized bending torque. The torque is bending beam and changing the incidence angle on the reflector surface – beam slope – in the vicinity of the actuator (see Figure 7). It is assumed that there is one incidence angle measurement per actuator. The feedback control goal is to compensate for the initial error in the reflector surface orientation by controlling the actuators.

The beam deflection $w(x)$, where x is the coordinate along the beam, and the beam middle line slope can be modeled as

$$C\frac{\partial^2 w}{\partial x^2} - Tw = Q, \qquad y = \frac{\partial w}{\partial x}, \tag{1}$$

where $Q(x)$ is the actuator bending moment. The spatial coordinate is assumed to be scaled such that the inter-actuator distance is unity. For building a control-oriented model, PDE (1) can be discretized as

$$\left(\lambda - 2 + \lambda^{-1}\right)w - \theta w = u, \qquad y = \frac{1}{2}\left(\lambda - \lambda^{-1}\right)w, \tag{2}$$

where λ is the spatial discrete Laplace variable corresponding to a unit spatial shift operator, $\theta = Q/C$ is a nondimensional beam tension parameter, and $u = Q/C$ is the control input.

The PDE (1) and the discretized equations (2) describe a static deflection of the beam. In reality a reflector beam with active shape control might have some structural damping, but would still experience structural vibrations under action of the changing control moment. To reduce the impact of the high-frequency vibrations observable through the sensor measurements, the sensor signal is assumed to pass through a first-order low-pass filter. The overall model follows and includes the filtering and dynamical uncertainty. This model has the form

$$y = P(\lambda)g(z)u + d\delta u\,, \tag{3}$$

$$P(\lambda) = -\frac{1}{2}\cdot\frac{\lambda^{-1}-\lambda}{\lambda^{-1}-(2+\theta)+\lambda}; \qquad g(z) = \frac{z^{-1}}{1-az^{-1}} \tag{4}$$

where $\delta = \delta(\lambda,z)$, $|\delta|\le 1$, is an unknown transfer function collecting the modeling errors; $d > 0$ is the uncertainty magnitude; $P(\lambda)$ is a spatial response operator defined by (4) with pulse response (Green function) in Figure 7; a is a dynamical exponential filtering factor. In the simulations, it was assumed that d= 0.2 (20% uncertainty is present in dynamic and spatial transfer function), a=0.8 (filter time constant is 4-5 samples), and θ = 0.3 (moderate tension in the beam).

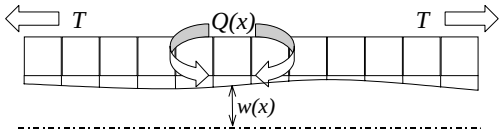

Figure 6: Schematics of a flexible reflector model

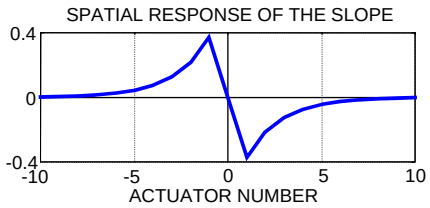

Figure 7: Spatial pulse response of the reflector slope corresponding to the operator $P(\lambda)$.

The controller for the system (3)—(4) was designed using a loopshaping technique similar to one discussed in [17]. The general form of the feedback controller is

$$(1-z^{-1})u = -c(z^{-1})K(\lambda)y - S(\lambda)z^{-1}u,, \tag{5}$$

$$c(z^{-1}) = k_P(1-z^{-1}) + k_I,, \tag{6}$$

where $K(\lambda)$ and $S(\lambda)$ are spatial operators and $c(z^{-1})$ is a dynamical PI feedback controller in velocity form. Non-causal spatial FIR operators $K(\lambda)$ and $S(\lambda)$ are designed such that the information from three closest neighbors on each side only is used for control of each actuator. The operator $K(\lambda)$ is chosen to equalize the loop gain across the controllable spatial frequencies while the operator $S(\lambda)$ is chosen to prevent large control action for the uncontrollable frequencies. These operators were designed based on the spatial operator $P(\lambda)$ in the plant (3). Such design allows for localized feedback control computations to be implemented in distributed control elements. In simulations below the following operators were used

$$\begin{aligned} K(\lambda) &= 0.0972\lambda^{-3} - 0.3110\lambda^{-2} + 1.4595\lambda^{1} + 0 + \\ &1.4595\lambda - 0.3110\lambda^{2} + 0.0972\lambda^{3} \\ S(\lambda) &= 0.1148\lambda^{-3} + 0.1636\,\lambda^{-2} - 0.3336\lambda^{-1} + \\ &0.6196 - 0.3336\lambda + 0.1636\,\lambda^{2} + 0.1148\lambda^{3} \end{aligned} \tag{7}$$

The PI dynamical feedback controller gains are k_P=0.15, k_I=0.07, such that a good quality of the transient process and disturbance rejection is achieved while the robustness is maintained in accordance with the specified 20% level of the uncertainty.

In accordance with [15], a structured uncertainty analysis of the closed-loop system (3), (4) with the controller (5)—(7) requires representing the system as a Linear Fractional Transform (LFT) with respect to the spatial, λ, and dynamical, z, Laplace variables and the uncertainty δ. As described in [22] this can be conveniently done by representing a system a an interconnection of simple blocks. Such block-diagram model of the closed-loop multidimensional system is shown in Figure 8. The diagram includes the uncertainty model in (3). The spatial and dynamical transfer functions g, P, c, K, S in the diagram are defined in (4), (6), and (7).

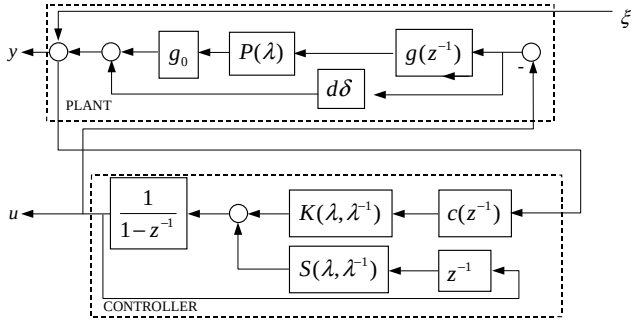

Figure 8: Block-digram of the closed-loop two-dimensional system. The system input is the external disturbance ξ. The control performance can be judged by how much this disturbance is suppressed in the system output y.

Following the approach of [15] to robust analysis of multidimensional systems, consider the requirement of spatial response localization for the closed-loop system in consideration. Demand that the closed-loop spatial response decays at least as fast as r^{-l} away from its center, where $r < 1$ is a localization parameter and l is the spatial coordinate distance from the response center. In the numerical example below r=0.8 was assumed. This means the response decays by an order of magnitude within 10 steps from its center. The response decay rate defines widths of boundary zones near the reflector bean ends. Outside of these boundary zones, the system behavior is closely approximated by the assumed 2-D model with an infinite spatial domain – infinite beam length.

The closed-loop stability in combination with spatial localization can be specified by computing a robust margin of the stability and localization that is given by a Structured Singular Value μ as discussed in [15]. The robust stability and localization conditions hold if $\mu < 1$ for all dynamical and spatial frequencies. The robust performance analysis results are shown in Figure 9. The Structured Singular Value μ in Figure 9 is plotted as a function of the dynamical and spatial frequency ratio to the respective Nyquist frequency (half the sampling rate). Since the plotted value is less that 0.66 at any combination of the frequencies, the closed loop system is robust to the dynamical uncertainty $\delta = \delta(\lambda,z)$ in (3) with a margin factor better than 50%. The analysis results show that the designed control can be safely implemented even though the design model (3) does not take flexible dynamics into account. After the low-lass filtering applied, these flexible dynamics are covered by the uncertain transfer function $\delta(\lambda,z)$ in the analysis.

An example of the closed-loop response with the controller (5)—(7) in compensation of random initial error is shown in Figure 10. Despite the fact that the actuator response has vanishing gain at small spatial frequencies, almost 80% of the initial error is canceled after first 10 control samples. These results shows that, though suboptimal, the designed distributed localized controller provides excellent performance and robustness of the antenna shape error compensation.

Conclusions

Effective surface precision control of future gossamer space reflectors will require large numbers of low-cost lightweight actuators. A multifunctional adaptive membrane concept is presented which meets these needs by embedding large numbers of actuators in the membrane using polymer based MEMS techniques. Polymer-MEMS are being proven today for many smart applications and are ready for development into an active surface. With distributed localized control, effective surface precision is maintained without massive complexity in the control systems. Only knowledge from local

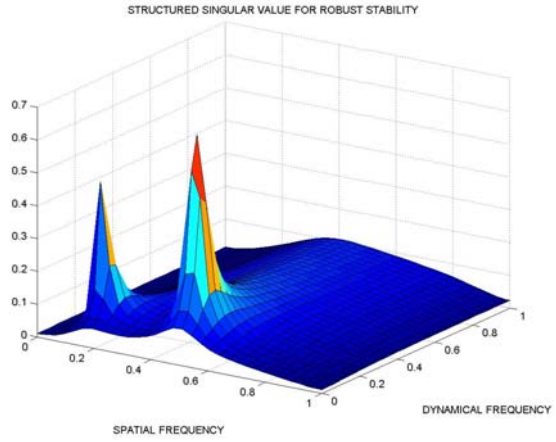

Figure 9: Generalized Structured Singular Value μ computed on a grid of dynamical and spatial frequencies.

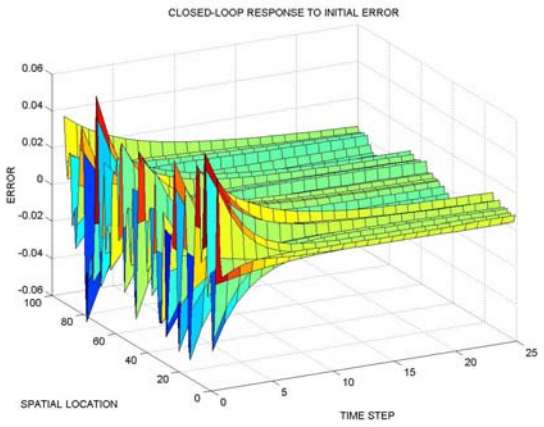

Figure 10: Simulation of initial error compensation.

and a few nearest neighbors is required. Expertise in this type of highly distributed localized control with many hundreds of actuators has been demonstrated in the industrial application of cross-directional process control. A highly controlled, precision reflector will be producible "by the yard" for inclusion in many deployable, inflatable, and free surface gossamer spacecraft concepts.

References

1. Moore, C. "Ultra-lightweight structures and observatories thrust area," *IEEE Aerospace Conference*, Big Sky, Montana, March 2000.
2. Chmielewski, A.B., Moore, C., Howard, R. "The gossamer initiative," *IEEE Aerospace Conference*, Big Sky, Montana, March 2000.
3. Montgomery E.E., "Variance of ultralightweight space telescope technology development priorities with increasing total aperture goals," *1999 Ultra Lightweight Space Optics Workshop,* Napa Valley, CA, March 1999
4. Chmielewski, A.B., Noca, M.A., Ulvestad, J. "ARISE antenna," *IEEE Aerospace Conference*, Big Sky, Montana, March 2000.
5. Njoku, E., Wilson, W., Yueh, S., Freeland, R., Helms, R., et al. "Large deployable-mesh antenna system for ocean salinity and soil moisture sensing," *IEEE Aerospace Conf.*, Big Sky, MT, March 2000.
6. Lake, M.S., Peterson, L.D., Mikulas, M.M., et al "Structural concepts and mechanics issues for ultra-large optical systems," *1999 Ultra Lightweight Space Optics Workshop,* Napa Valley, CA, March 1999
7. Cabuz, C., Cabuz, E.I., Ohnstein, T.R., Neus, J., Maboudian, R. "Factors enhancing the reliability of touch-mode electrostatic actuators," *Sensors and Actuators*, Vol. 79, 2000, pp. 245-250.
8. Cabuz, C., Cabuz, E.I., Rolfer, T., Herb, W., Zook, D. "Mesoscopic sampler based on 3d array of electrostatically activated diaphragms," *10th Int. Conf. on Solid-State Sensors and Actuators, Transducers'99*, June 7-12, 1999, Sendai, Japan
9. Horning, R., Johnson, B. "Polymer-based MEMS actuators for biomimetics", *Neurotechnology for Biomimetic Robots*, 14-16 May, 2000
10. US Patent 5,836,750, *Electrostatically Actuated Mesopump Having a Plurality of Elementary Cells* (C. Cabuz)
11. US Patent 6,179,586, *Dual Diaphragm, Single Chamber Mesopump* (Herb, Zook, Cabuz)
12. Duncan, S.R, Dumont, G.A., and Gorinevsky, D.M. "Evaluating the performance of cross-directional control systems," *American Control Conf.*, San Diego, CA, June 1999
13. Gorinevsky, D. and Heaven, M. "Performance-optimized identification of cross-directional control processes," *IEEE Conf. on Decision and Control*, San-Diego, CA, Dec. 1997, pp. 1872—1877; to appear in *IEEE Tr. on Automatic Control*.
14. Gorinevsky, D., Heaven, M., and Vyse, B. "Performance analysis of cross-directional process control," *IEEE Tr. on Control Systems Technology*, vol. 8, no. 4, July 2000, pp. 589—600.
15. Gorinevsky, D., and Stein G., "Structured uncertainty analysis of robust stability for spatially distributed systems," *39th IEEE Conf. on Decision and Control*, Sydney, Australia, December 2000.
16. Gorinevsky, D., and Stein G., "Uncertainty models for control of distributed actuator and sensor arrays," SPIE Paper #3984-50, *SPIE 7th Annual Intern. Symposium on Smart Structures and Materials*, 5-9 March 2000, Newport Beach, CA
17. Stewart, G., Gorinevsky, D., and Dumont, G. "Design of a practical robust controller for a sampled distributed parameter system," *37th IEEE Conf. on Decision and Control*, Tampa, FL, Dec. 1998.
18. Stewart, G.E., Gorinevsky, D., and Dumont, G.A., "H_2 loopshaping controller design for spatially distributed systems," *IEEE Conference on Decision and Control*, Phoenix, AZ, December 1999
19. Bamieh, B., Paganini, F., and Dahleh, M. "Distributed control of spatially-invariant systems," *IEEE Trans.on Automatic. Contr.*, 2000.
20. Bose, N.K. *Applied Multidimensional Systems Theory*, Van Nostrand Reynhold, 1982.
21. Stewart, G.E., Gorinevsky, D., and Dumont, G.A., "Spatial loopshaping: A case study on cross-directional profile control," *American Control Conf.*, pp. 3098—3103, San Diego, CA, June 1999.
22. Zhow, K., Doyle, J., and Glover, K., *Robust and Optimal Control*, Prentice Hall, 1999